DINAME 2023 - Proceedings of the XIX International Symposium on Dynamic Problems of Mechanics,
A.S. De Paula, A.T. Fabro and M.R. Machado (Editors), ABCM.
Pirenópolis, Go, Brazil, February 26th to March 3rd, 2023

# Configuration of aerodynamics model in flight simulator to investigate Pilot-Induced Oscillations and Loss of Control

**Juliano A. B. Gripp [1], Marco A. G. Moreira [2], Luís G. Trabasso [3], and Cleverson M. P. Marinho [4]**

[1,2,4] EMBRAER. Rod. Pres. Dutra, km 134, São José dos Campos, SP, 12247-820, Brazil

[3] ISI – Instituto SENAI de Inovação. R. Arno Waldemar Döhler, 308, Joinville, SC, 89218-153, Brazil

*Abstract: Consistently over the years, Pilot-Induced Oscillations (PIO) and Loss Of Control In-flight (LOC-I) have been contributing factors for aircraft incidents. Some initiatives around the world to mitigate issues like PIO and LOC-I and comply with rigorous recommendations from aviation regulatory agencies involve improvements in modeling, simulation, and training of flight crew. In this sense, EMBRAER and Instituto Tecnológico de Aeronáutica (ITA) have developed alternatives for pilot training in a high-fidelity environment for flight simulation, for example SIVOR: a flight simulator assisted by a robotic motion platform. In order to study representative flight conditions, propose flight control laws and allow unclassified publication of results, a "open-source" aerodynamics model of a transport aircraft was configured into SIVOR, as well as the simulation environment. This paper presents main steps of configuration, from aerodynamics model build-up in Simulink up to validations with pilot-in-the-loop. It was possible to define a process for setup of aerodynamics models in order to allow the SIVOR platform to be collaborative and flexible for new designs and research.*

***Keywords: Robotics and Mechatronic Systems, Aircraft Modeling, Control Systems, Pilot-Induced Oscillation, Loss of Control***

## INTRODUCTION

Pilot-Induced Oscillation (PIO) problem has been present in aviation throughout the history of manned flight. PIOs have caused numerous accidents with results ranging from minor damage to total loss of the aircraft and pilot (Klyde et al. (1995)) and it is still a challenging topic of recent works such as Efremov et al. (2020). The military standard MIL-STD-1797B (USAF, 2006) defines PIO as "sustained or uncontrollable oscillations resulting from efforts of the pilot to control the aircraft".

Consistently over the years, Loss of Control In-flight (LOC-I) has been one of the leading causes of crashes and fatalities (Boeing (2020)). LOC-I is defined as "loss of aircraft control while, or deviation from intended flight path, in flight". Loss Of Control In-Flight is an extreme manifestation of a deviation from intended flight path. References have been investigating alternatives to cope with LOC-I, for example designing flight control laws to prevent and recover the aircraft in case of Loss of Control (Belcastro (2012)).

Motivated by the challenge to minimize occurrences of PIO and LOC-I in aircraft, industry and academy have joined efforts to develop alternatives for pilot training in a high-fidelity environment for flight simulation, in order to comply with rigorous recommendations from aviation regulatory agencies, in terms of modeling, simulation, and training of flight crew. In this way, EMBRAER and Instituto Tecnológico de Aeronáutica (ITA) have developed SIVOR ("*Simulador de Voo com base Robótica de Movimento*"): a flight simulator assisted by a robotic motion platform (Silva et al. (2019)).

In order to study representative flight conditions, propose flight control laws and allow publication of results without expose restrict data from aircraft, a "open-source" aerodynamics model of a large cargo transport aircraft was configured into SIVOR, as well as the simulation environment. This paper highlights as contribution the documentation and insights of main steps for configuration, from aerodynamics model build-up in Simulink (whose data were extracted from NASA and Boeing reports available in literature), up to validations with pilot-in-the-loop. Next sections present a process for integration of aerodynamics models in order to allow the SIVOR platform and other similar ones to be collaborative and flexible to adapt different airframes and configurations.

## INTEGRATION OF AIRCRAFT MODEL

### *Overview of aircraft and aerodynamics model*

For design of representative flight control laws and research in the context of PIO and LOC-I, it is necessary to have detailed information about the aircraft. Considering the level of details from report such as NASA (1970), the airframe of the aircraft Boeing 747-100 (four-fanjet intercontinental transport aircraft) was adopted for this study. Figure 1 presents a schematic view of the aircraft, highlighting the control surfaces and some characteristics. Directional (yaw)

control is obtained from two rudder segments (upper and lower rudder). Lateral control system consists of inboard ailerons (High Speed Ailerons), outboard ailerons (Low Speed Ailerons) and roll spoilers. Longitudinal control is given by horizontal stabilizer, inboard elevators, and outboard elevators.

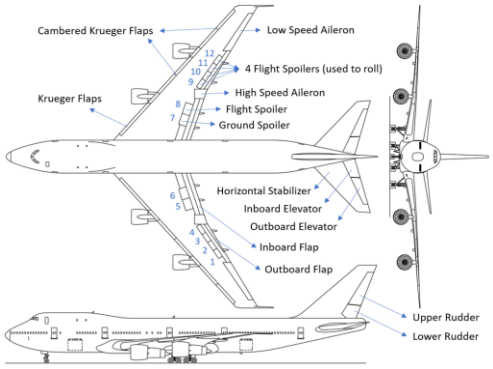


| | |
|---|---|
| MTOW | 323 ton / 712 klb |
| Engines | 4x fanjet |
| Max Range | 9800 km |
| Ceiling | 45 kft |
| Cruise Speed | 523 kt |
| Wing span | 60 m |
| Length | 70 m |
| Ailerons | 2 inner, 2 outer |
| Rudders | 1 upper, 1 lower |
| Roll Spoilers | 4 in each wing |
| Flaps | 0 a 30 deg |

**Figure 1 – Views of Boeing 747-100 and some characteristics.**

Data available in the report NASA (1970) regarding to aerodynamics model (databank) has high level of information, but it is presented in low-quality figures, describing the behavior of aerodynamic coefficients as function of angle of attack, altitude, Mach number, flap settings, among other parameters. For example, Equation 1 illustrates the definition of the dimensionless aerodynamic lift force coefficient ($C_L$) provided by NASA (1970) at a given $\alpha_{WDP}$ (angle-of-attack at wing design plane), which is shifted 2 deg from angle-of-attack at the fuselage reference line ($\alpha$).

$$\begin{aligned} C_L = C_{L\_Basic\{\delta Flap,\ Mach,\ \alpha WDP\}} + \Delta C_{L\_elasticity\{\delta Flap,\ EAS,\ Mach,\ Alt\}} + \left[\Delta(dC_L/d\alpha)_{\{\delta Flap,\ EAS,Mach,Alt\}}\right] \alpha_{WDP} + \\ \left[(dC_L/d\alpha')_{\{\ Mach\}}\right](\alpha'\ c/(2\ V_{TAS})) + \left[(dC_L/dq)_{\{\ Mach,\ Alt,\ CG\}}\right](q\ c/(2\ V_{TAS})) + \left[(dC_L/dn_z)_{\{\ \delta Flap,\ EAS,\ Mach,\ Alt\}}\right] n_z + \\ K_{\alpha\{\delta Flap,\ \alpha WDP\}}\left[(dC_L/dHstab)_{\{\ Mach,Alt\}}\right] \delta Hstab + K_{\alpha\{\delta Flap,\ \alpha WDP\}}\left[(dC_L/de_i)_{\{Mach,Alt\}}\right] \delta e_i + \\ K_{\alpha\{\delta Flap,\ \alpha WDP\}}\left[(dC_L/de_o)_{\{Mach,Alt\}}\right] \delta e_o + \Delta C_{L\_spoilers\{spoilers,\delta Flap,\ Mach,\ \alpha WDP,Alt,hAGL\}} + \\ \Delta C_{L\_ailerons\_outboard\{ailerons\ outboard,\delta Flap,\ \alpha WDP\ \}} + \Delta C_{L\_landing\_gear\{gear\ position,\delta Flap,\ \alpha WDP,\ Mach\}} + \Delta C_{L\_ground\_effect\{\ \delta Flap,\ \alpha WDP,\ hAGL\}} \end{aligned} \quad (1)$$

where "$C_L$" is lift coefficient, "Mach" is Mach number, "EAS" is Equivalent Airspeed, "Alt" is Pressure Altitude, "$h_{AGL}$" is altitude above ground level, "c" is mean aerodynamic chord, "$V_{TAS}$" is true airspeed, "CG" is center of gravity, "$q$" is pitch rate, "$n_z$" is load factor, "$K_\alpha$" is a normalized factor, "Hstab" is horizontal stabilizer, "e" is elevator. The notation $\delta$ indicates deflection of control surfaces, $\Delta$ indicates change in basic lift coefficient due to change in certain variable, $\alpha'$ represents time derivative of $\alpha$, {.} indicates what is necessary to calculate each term. For example $C_{L\_Basic\{\delta Flap,\ Mach,\ \alpha WDP\}}$ depends on flap position ($\delta$Flap), Mach number, and $\alpha_{WDP}$ to be calculated.

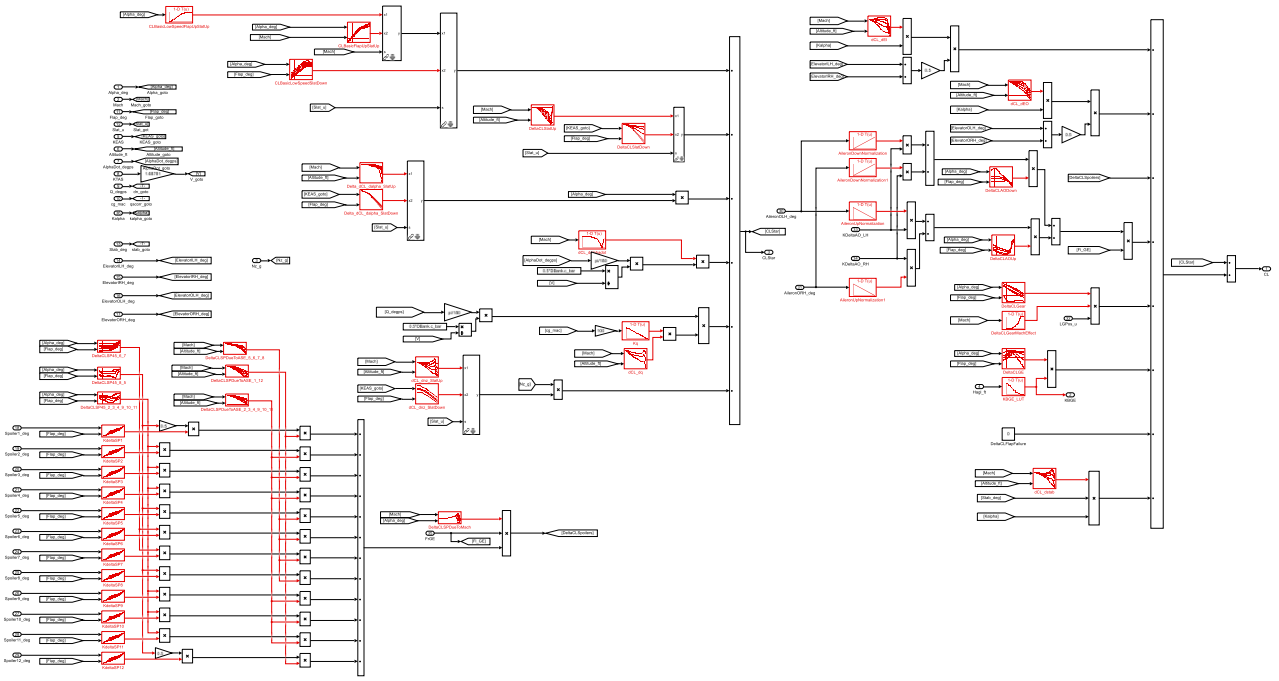

**Figure 2 – Example of Lift Coefficient (CL) modeling in Simulink. Look-up tables highlighted in red color.**

Figure 2 illustrates the implementation of lift force coefficient ($C_L$) in Simulink software following description of Equation 1, where each lock-up table is represented by a red box. Similar process was conducted for other aerodynamics coefficients as well: Drag Force ($C_D$), Pitching Moment ($C_M$), Lateral Force ($C_y$), Rolling Moment ($C_\ell$), Yawing Moment ($C_n$). Approximately 250 figures of tables like the presented in Figure 3 were converted into Simulink Look-up tables (red boxes as presented in Figure 2) to compose the equations of the aerodynamics model.

### *Validation of the integrated model in Simulink*

Following the equations from report NASA (1970) which describe the relations of forces and moments involving aerodynamic coefficients for Drag Force ($C_D$), Lift Force ($C_L$), Pitching Moment ($C_M$), Lateral Force ($C_y$), Rolling Moment ($C_\ell$), Yawing Moment ($C_n$), it was possible to integrate the aerodynamics model with other models for "Engine", "Equations of Motion", and "Atmosphere". That integration, illustrated in Figure 3, allows analysis of bare-airframe, trimming in defined flight conditions, generation of linear models around trimmed conditions as well as simulation of basic maneuvers (open-loop, without flight control law at this phase). Figure 3 shows examples of images with plots of aerodynamic coefficients whose data were converted into look-up tables at Simulink software.

"Engine" model was implemented according to description in the report NASA (1970); "Atmosphere" model is based on International Standard Atmosphere (ISA), and "Equations of Motion" describes traditional six degrees of freedom equations for forces and moments (Steven and Lewis (1992)). In Figure 3 the acronyms "ATM", "F", "M", "EQM", "eng", "aero", "grav" stand for Atmosphere model, Force, Moment, Equation of Motion model, Engine model, aerodynamics databank and gravity, respectively. The model inputs are Throttle, deflection of Actuators (ailerons, roll spoilers, rudder, elevator) and Mass Properties (Mass and Center of Gravity, CG). The main outputs are aircraft velocity (V), Pressure Altitude (Alt), angular rates ($p$, $q$, $r$), accelerations at CG (ax, ay, az), Euler angles ($\phi$, $\theta$, $\psi$) and aerodynamic angles ($\alpha$, $\beta$, $\gamma$).

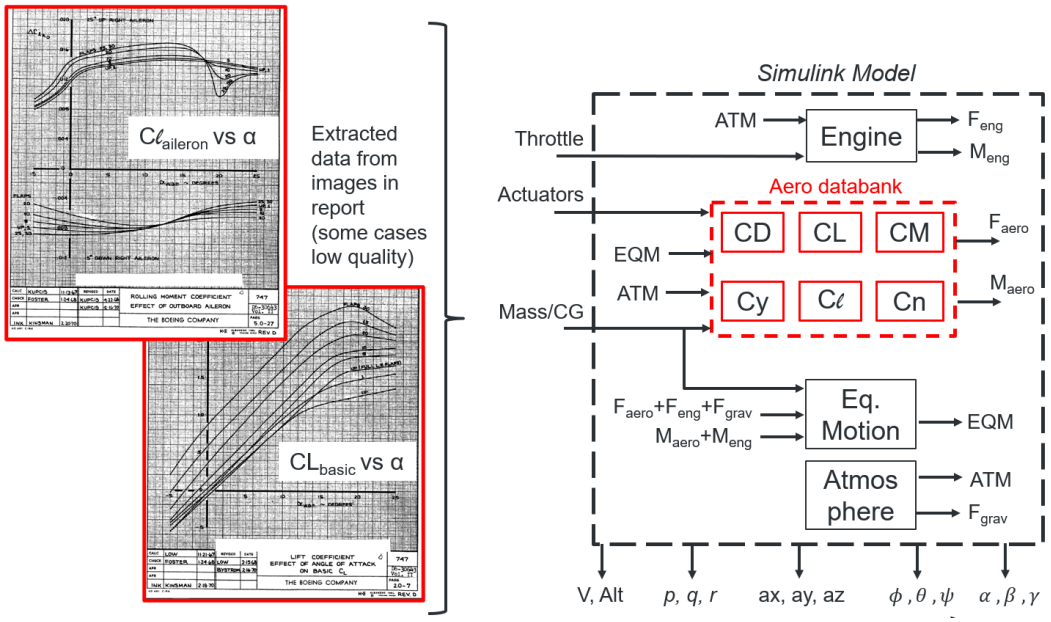


**Figure 3 – Data extracted from NASA (1970) to build-up model for trim and linearization in Simulink.**

Simulations of the model presented in Figure 3 were validated, by comparing trim results with trim examples provided by report NASA (1970). Table 1 shows results for different combinations of flap deflection, landing gear position. Mass, CG (center of gravity), Pressure altitude, Indicated Airspeed, Mach number, flight path angle (gamma, $\gamma$). For example, pitch angle ($\theta$) and horizontal stabilizer deflection (Hstab) were compared. Columns "$\theta$ [deg] (Boeing)" and "$\theta$ [deg] (NASA)" present reference values provided by Boeing and NASA, whereas "$\theta$ [deg] (model)" present data obtained from integrated model in trimming process (Figure 3). Column "$\theta$ error to average [deg]" gives the absolute error between "$\theta$ [deg] (model)" and the mean value of "$\theta$ [deg] (Boeing)" and "$\theta$ [deg] (NASA)". Similar analysis is presented for Hstab, comparing data from model and data from report NASA (1970). In general, it is possible to check that the integrated model matches very well with data from report NASA (1970), which validates the integration process.

Additionally, independent spot checks were performed to compare derivative of aerodynamic coefficients given by the aerodynamics model versus examples presented in the book Roskam (1985). For example, assuming the flight condition Flap=30deg, Calibrated Airspeed=130kn, Altitude=100ft, $\alpha_{WDP}$=10.5deg, Mass=564klb, CG=25%MAC, the numeric derivative of $Cn_\beta$ is presented in Figure 4(b), which corresponds to derivative of curve Cn vs β (Figure 4(a)) at $\alpha_{WDP}$=8.5deg and β=0deg. The value 0.187rad$^{-1}$ matches with the value presented in Roskam (1985): 0.184. Similar analysis is presented in Table 2 for other aerodynamic derivatives.

**Table 1 – Comparison of trim results for integrated model versus data from Boeing and NASA (NASA (1970)).**

| Comparison Case | Flap [deg] | Landing Gear | Mass [x1000 lb] | CG (% MAC) | Pressure Altitude [x1000 ft] | Indicated Airspeed [kn] | Mach [-] | Gamma [deg] | θ [deg] (Boeing) | θ [deg] (NASA) | θ [deg] (model) | **θ error to average [deg]** | Hstab [deg] (Boeing) | Hstab [deg] (NASA) | Hstab [deg] (model) | **Hstab error to average [deg]** |
|---|---|---|---|---|---|---|---|---|---|---|---|---|---|---|---|---|
| 1 | 0 | Up | 650 | 12 | 20 | 373 | 0.80 | 0.0 | 0.30 | 0.21 | 0.32 | 0.06 | -0.60 | -0.49 | -0.49 | 0.06 |
| 2 | 0 | Up | 650 | 32 | 20 | 373 | 0.80 | 0.0 | 0.10 | 0.02 | 0.12 | 0.06 | 0.60 | 0.63 | 0.65 | 0.03 |
| 3 | 0 | Up | 500 | 14 | 20 | 373 | 0.80 | 0.0 | -0.70 | -0.67 | -0.58 | 0.11 | -0.10 | -0.05 | -0.04 | 0.03 |
| 4 | 0 | Up | 500 | 14 | 20 | 275 | 0.60 | 0.0 | 2.00 | 1.96 | 1.95 | -0.03 | -1.30 | -1.24 | -1.25 | 0.02 |
| 5 | 0 | Up | 500 | 14 | 35 | 253 | 0.75 | 0.0 | 2.40 | 2.29 | 2.33 | -0.02 | -1.80 | -1.71 | -1.75 | 0.01 |
| 6 | 0 | Up | 500 | 14 | 35 | 295 | 0.86 | 0.0 | 0.70 | 0.59 | 0.59 | -0.06 | -1.30 | -1.20 | -1.17 | 0.08 |
| 7 | 0 | Up | 500 | 32 | 35 | 253 | 0.75 | 0.0 | 2.10 | 2.01 | 2.05 | -0.01 | -0.10 | -0.09 | -0.09 | 0.01 |
| 8 | 0 | Up | 500 | 32 | 35 | 295 | 0.86 | 0.0 | 0.50 | 0.40 | 0.39 | -0.06 | -0.10 | 0.00 | 0.04 | 0.09 |
| 9 | 0 | Up | 500 | 32 | 35 | 318 | 0.92 | -1.7 | -1.20 | -1.48 | -1.44 | -0.10 | 0.00 | 0.08 | -0.02 | -0.06 |
| 10 | 10 | Up | 550 | 15 | 5 | 167 | 0.28 | 0.0 | 8.10 | 8.05 | 7.94 | -0.13 | -4.80 | -4.72 | -4.72 | 0.04 |
| 11 | 20 | Up | 550 | 15 | 5 | 159 | 0.26 | 0.0 | 6.50 | 6.48 | 6.37 | -0.12 | -5.50 | -5.40 | -5.44 | 0.01 |
| 12 | 25 | Down | 550 | 15 | 5 | 155 | 0.26 | 0.0 | 5.90 | 5.82 | 5.80 | -0.06 | -5.60 | -5.52 | -5.55 | 0.01 |
| 13 | 25 | Down | 550 | 15 | 5 | 135 | 0.22 | 0.0 | 9.70 | 9.59 | 9.60 | -0.04 | -7.90 | -7.85 | -7.90 | -0.03 |
| 14 | 30 | Down | 550 | 15 | 5 | 150 | 0.25 | 0.0 | 3.80 | 3.75 | 3.76 | -0.02 | -6.20 | -6.19 | -6.16 | 0.03 |
| 15 | 10 | Up | 710 | 11 | 5 | 190 | 0.32 | 0.0 | 8.40 | 8.41 | 8.28 | -0.12 | -5.60 | -5.52 | -5.48 | 0.08 |
| 16 | 10 | Up | 710 | 32 | 5 | 190 | 0.32 | 0.0 | 7.80 | 7.80 | 7.64 | -0.16 | -0.90 | -0.81 | -0.83 | 0.02 |
| 17* | 30 | Down | 564 | 15 | 0 | 142 | 0.22 | 0.0 | 5.70 | 5.53 | 4.04 | -1.58 | -7.50 | -7.37 | -8.76 | -1.32 |
| 18* | 30 | Down | 564 | 33 | 0 | 142 | 0.22 | 0.0 | 5.00 | 4.86 | 3.24 | -1.69 | -1.90 | -1.86 | -3.18 | -1.30 |
| 19 | 30 | Down | 564 | 15 | 10 | 142 | 0.26 | 0.0 | 5.70 | 5.52 | 5.54 | -0.07 | -7.60 | -7.44 | -7.52 | 0.00 |
| 20 | 30 | Down | 564 | 15 | 10 | 180 | 0.33 | 0.0 | 0.20 | 0.21 | 0.17 | -0.04 | -3.70 | -3.65 | -3.73 | -0.05 |
| 21 | 25 | Down | 564 | 15 | 10 | 180 | 0.33 | 0.0 | 3.10 | 3.10 | 3.06 | -0.04 | -3.80 | -3.79 | -3.82 | -0.02 |
| 22* | 30 | Down | 400 | 15 | 0 | 120 | 0.18 | 0.0 | 5.30 | 5.14 | 3.53 | -1.69 | -7.40 | -7.30 | -8.61 | -1.26 |

*Model adopts "Revised Data" from section 19 in the cases 17, 18, 22

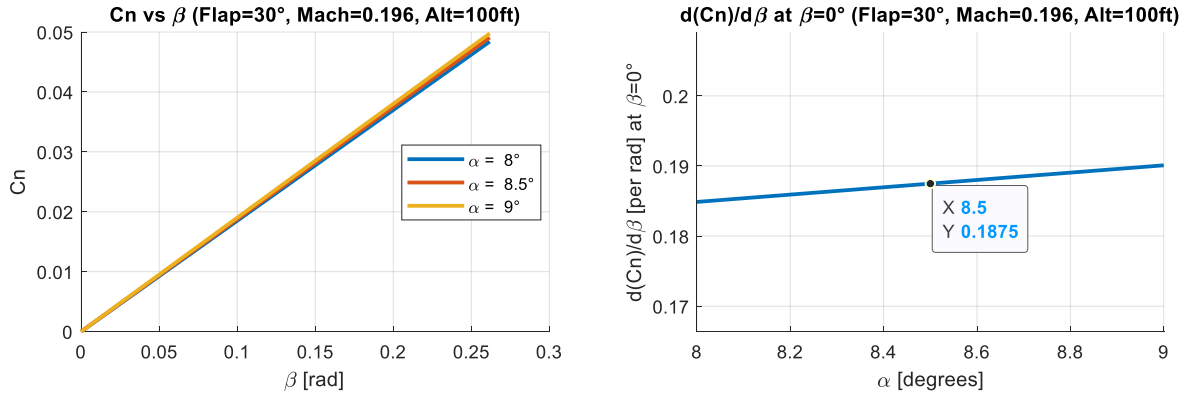


**Figure 4 – (a) Example of Cn versus β. (b) Example of derivative $Cn_\beta$, for α=8.5° ($\alpha_{WDP}$=10.5°).**

**Table 2 – Examples of comparison for aerodynamic derivatives of integrated model versus data from Roskam (1985). Trim case: Flap=30deg, Calibrated Airspeed=130kn, Alt.=100ft, $\alpha_{WDP}$=10.5deg, Mass=564klb, CG=25%MAC**

| Aerodynamic Derivative [rad$^{-1}$] | Symbol | Roskam (1985) | Model |
|---|---|---|---|
| Derivative of Rolling moment due to roll rate | $C\ell_p$ | -0.502 | -0.519 |
| Derivative of Yawing moment due to sideslip angle | $Cn_\beta$ | 0.184 | 0.187 |
| Derivative of Yawing moment due to yaw rate | $Cn_r$ | -0.360 | -0.370 |
| Derivative of Yawing moment due to rudder deflection | $Cn_{\delta rud}$ | -0.113 | -0.111 |

Finally, additional spot checks were performed to compare linear models trimmed around certain conditions with linear models obtained from an independent model for same aircraft: RECOVER (2019). In all checks that were performed, integrated model presents good matching and representation.

### *Flight Simulator overview*

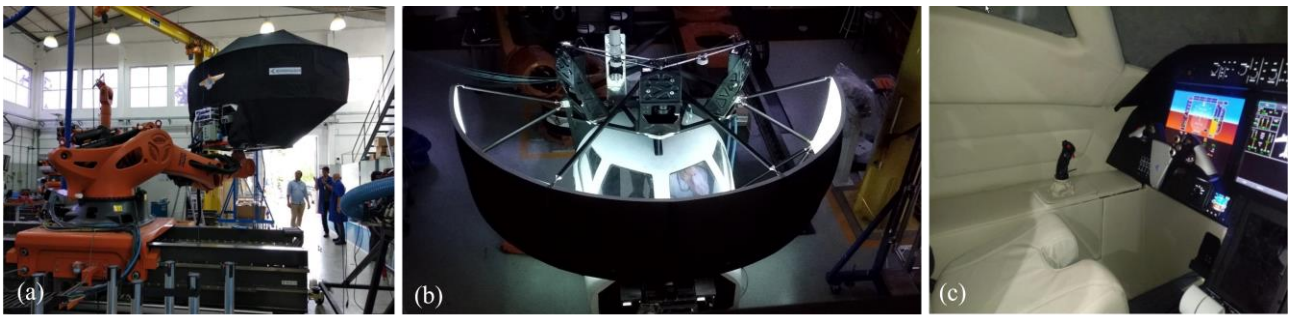


**Figure 5 - External and internal views of SIVOR Flight Simulator, Silva et al. (2019), Oliveira et al. (2019).**

For this work, a flight simulator assisted by a robotic motion platform (called "SIVOR", acronym for "*Simulador de Voo com Plataforma Robótica de Movimento*"), installed at ITA ("Instituto Tecnológico de Aeronáutica", Brazil) facilities was selected as platform for tests. SIVOR simulator is a motion-based flight simulator under development at ITA in partnership with Embraer company (Oliveira et al. (2019), Silva et al. (2019)). The SIVOR robot, a "KUKA KR-Titan", has a payload of 1,000 kg, making it possible to carry a high-fidelity cabin of a small aircraft, as illustrated in Figure 5. For sake of scope reduction, without compromising conclusions of this work, the tests with pilots were conducted like in a usual fixed-base flight simulator (i.e., motion disabled). Although the selected airframe corresponds to Boing 747-100, sidesticks (Figure 5(c)) were adapted as lateral inceptors for flight simulations, facilitating investigations of PIO for example. Other important available inceptors for this test are rudder pedals, throttle levers, flap levers.

### *Integration of models in flight simulator*

Considering the validated model integration presented in Figure 3, and the architecture of designed flight simulator (Figure 5), extra models for "Actuators" and "Sensors" were considered, in order to define closed-loop control systems for design of flight control laws.

For the modeled system, the properties of the actuators are summarized in the Table 3, such as cross-over frequency ($\omega_c$) and damping ratio ($\zeta$), considering a representation as second-order systems.

**Table 3 – Actuators' properties, adapted from NASA (1970), Silva (2009).**

| Actuator | $\omega_c$ [rad/s] | $\zeta$ [-] | Negative Limit [deg] | Positive Limit [deg] | Rate Limits [deg/s] |
|---|---|---|---|---|---|
| Aileron | 31.4 | 0.7 | -25 (up) | +20 (down) | ±50 |
| Roll Spoiler | 31.4 | 0.7 | 0 (closed) | +45 (up) | ±75 |
| Rudder | 31.4 | 0.7 | -25 (yaw to right) | +25 (yaw to left) | ±50 |
| Elevators | 31.4 | 0.7 | -23 (up) | +17 (down) | ±37 |

The properties of the sensors are summarized in the Table 4, such as cross-over frequency ($\omega_c$) and damping ratio ($\zeta$), considering a representation as second-order systems for some sensors or pure transport delay in other cases. Additionally, each sensor signal has a Transport delay, to account for sampling skew and bus transport delays. Moreover, the computation delay upstream of each actuator is set to 10 ms, assuming that the Flight Control Compute runs at 100 Hz .

**Table 4 – Sensors' properties, adapted from NASA (1970), Silva (2009).**

| Signal | Meaning | $\omega_c$ [rad/s] | $\zeta$ [-] | Transport Delay [ms] |
|---|---|---|---|---|
| $\phi$ | Euler roll angle | - | - | 30 |
| $\theta$ | Euler pitch angle | - | - | 30 |
| $\psi$ | Euler yaw angle | - | - | 30 |
| $p$ | Roll Rate in body axis | 50.3 | 0.7 | 27 |
| $q$ | Pitch Rate in body axis | 50.3 | 0.7 | 27 |
| $r$ | Yaw Rate in body axis | 50.3 | 0.7 | 27 |
| ax | Longitudinal Acceleration at CG | 50.3 | 0.7 | 27 |
| ay | Lateral Acceleration at CG | 50.3 | 0.7 | 27 |
| az | Normal Acceleration at CG | 50.3 | 0.7 | 27 |
| $\alpha$ | Angle of attack | - | - | 85 |
| $\beta$ | Angle of sideslip | - | - | 85 |

Examples of variables to be regulated by control laws are angle of attack ($\alpha$), pitch rate ($q$), load factor ($N_z$), roll rate ($p$) and sideslip angle ($\beta$). References such as Moreira et al. (2022) describe longitudinal control laws for $\alpha$, $q$ and $N_z$ using the integrated aircraft model (Figure 3), whereas the reference Gripp et al. (2023a) describes lateral-directional control laws for $p$ and $\beta$ (Beta) using same aircraft model.

With designed controls laws for the aircraft adopted as case study, additional models might be integrated in order to improve the fidelity of flight simulator. For example, "Displays" provide indications for flight crew such as speed, altitude, attitude. "Visual" model provides data to a commercial software (for example *X-Plane* or *Flight Gear*) which interprets aircraft attitude in terms of Euler angles and provide images to "Projectors", to be projected in front of the cabin, giving to pilot the sense of immersion in flight.

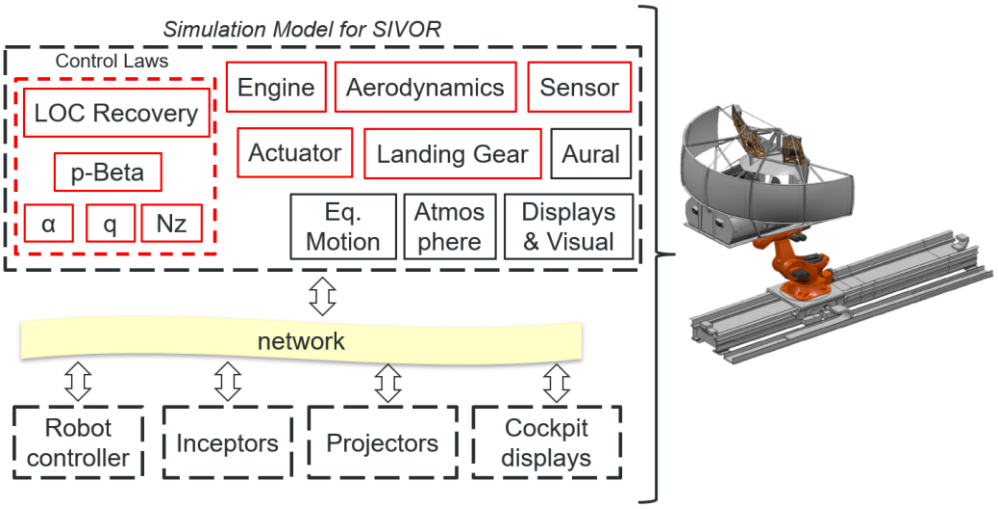


**Figure 6 – Overview of SIVOR environment for flight simulation (in red, necessary changes for each aircraft).**

Figure 6 presents an overview for integration of models adopted in SIVOR flight simulator. "Landing Gear" model is necessary to evaluate transitions air-ground and check dynamics of landing gear extraction/retraction, but it was not explored in this integration. All the models presented in the top portion of figure ("Simulation Model for SIVOR") are compiled together from Simulink and interact with other models of other suppliers ("Robot Controller", "Inceptors", "Projectors", "Cockpit displays") using a shared network. "Robot Controller" model receives position and acceleration from simulation model in order to position the robotic arm, providing motion to the whole cabin if necessary. "Inceptors" represent a controller for sidestick, pedals, yoke or column, depending on the necessary commands for aircraft under analysis. Inceptors must be calibrated in terms of deflection and force to represent compatible commands that pilot are used to exercise. "Cockpit displays" are fed by "Displays" model to draw the avionics symbols for pilot on the screen.

Additional indications on the Primary Flight Display (PFD) or aural annunciations can be considered depending on the purpose of test in flight simulator. For example, in terms of LOC-I investigations, it could be useful to plot indications on the PFD to alert the pilot that certain undesirable condition was achieved, or a recovery control law was engaged for example, increasing situational awareness.

In order to check the characteristics of aircraft and flight control laws in the context of PIO, for example, it might be valuable to show indications for the pilot to track, forcing the Pilot-Vehicle System to enter in possible PIO prone conditions. The proposed methodology was to perform some tracking tasks with different profiles. A target symbol (flight director) was programmed to display on the PFD a tracking reference for the pilot (Figure 7). In practical terms, the pilot task is to track as much and quick as possible the flight director in PFD (magenta symbol in Figure 7). Current flight path is represented by green symbol in Figure 7.

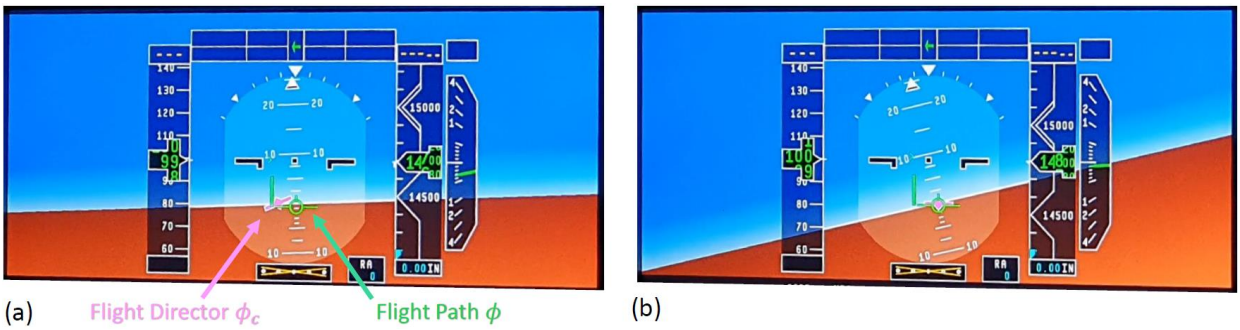


**Figure 7 - Screenshots of PFD. (a) Pilot looking for tracking. (b) Target tracked.**

Other traditional indications are depicted as well on the PFD (Figure 7): speed tape at left side (in knots), altitude tape at right side (in feet), horizontal markers in white to indicate pitch angle or angle of attack (in degrees), inclination markers on top semi-circle to indicate roll angle (in degrees).

## TESTS WITH PILOT-IN-THE-LOOP

The integrated model presented in Figure 6 was tested successfully by two pilots with large experience in different classes of aircraft in order to check representativeness of flight simulation, in terms of flight controls, control laws, human factors, ergonomics, avionics symbology, visual cues, just to cite some aspects. Figure 8 illustrates general tests of pilots in SIVOR flight simulator.

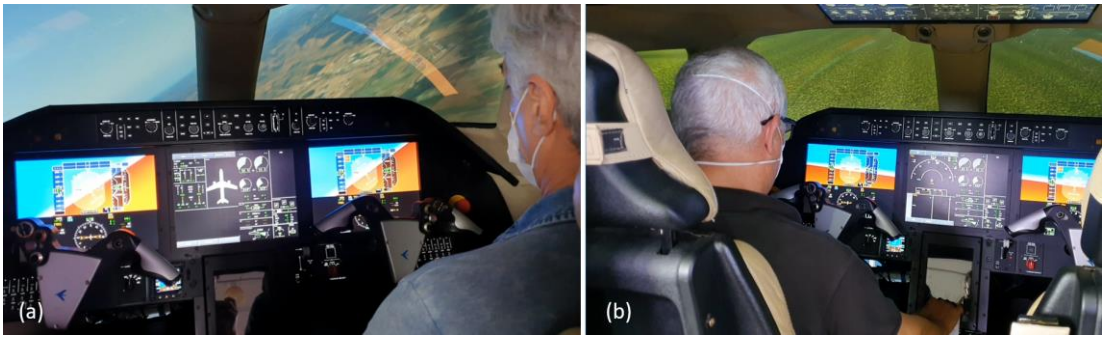


**Figure 8 – Validation of integrated model in SIVOR with pilot-in-the-loop.**

Even though many validations have been performed before flight tests with pilot-in-the-loop, pilot evaluation is essential to check *consistence* of simulation (signs of commands, smoothness, amplitudes), no *irregularities* such as significant discontinuities or "dead zones", as well as flying qualities. Besides general feedbacks from pilots to improve the simulation environment, a particular set of maneuvers was selected to check with pilots the integration of "Simulation Model for SIVOR" and the flight control laws:

- "bank capture" (from straight level flight rapidly roll the aircraft to one side using a step command input, in order to achieve 30 degrees of inclination, bank angle; then repeat process to capture minus 30 degrees);
- "pitch capture" (from straight level flight rapidly pitch down the aircraft, in order to achieve minus 10 degrees of pitch; then repeat process to capture plus 10 degrees of pitch);
- "Offset landing" (pilot tracks the glideslope and localizer during landing approach, with a lateral offset of 150 m, upon reaching 300ft above ground level, called out by the test engineer, he corrects to set up for landing, ensuring that the aircraft is wings level at threshold crossing on the centerline);
- "synthetic task" (marker in primary flight display was drawn for pilot to track as reference, changing bank angle and pitch angle).

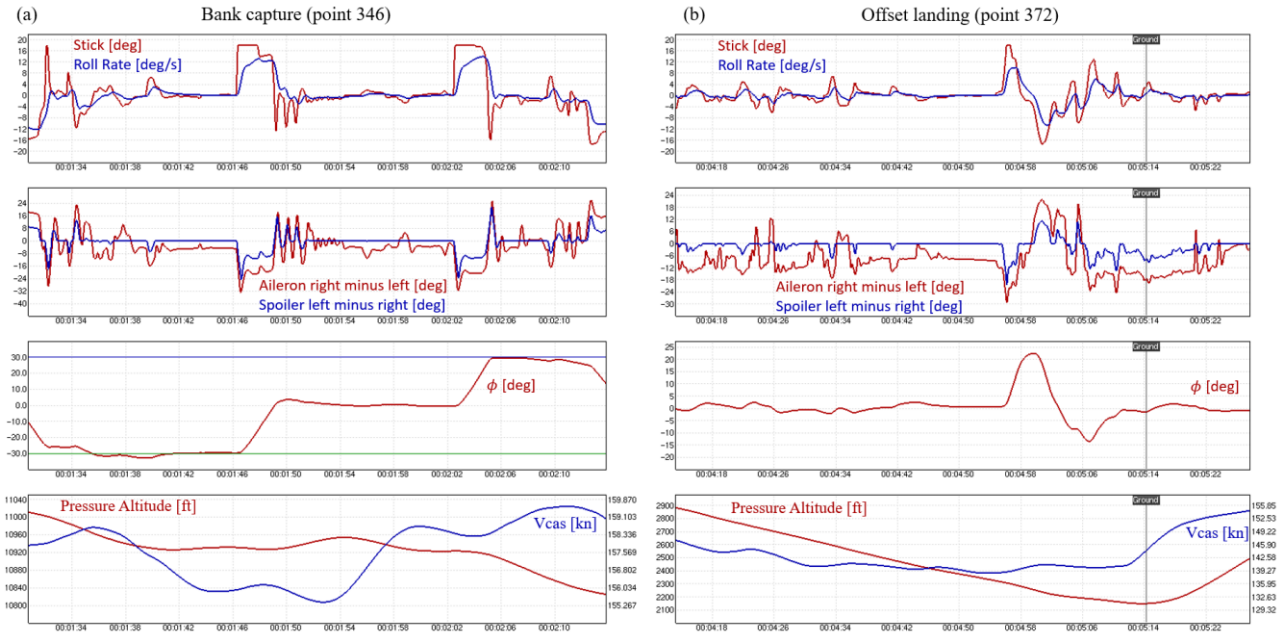


**Figure 9 – Ex. maneuvers performed by Pilot B at SIVOR (17/dec/2022). (a) Bank capture ±30°. (b) Offset landing.**

For illustration, Figure 9 presents time histories for maneuvers of bank capture (a) and offset landing (b). It is interesting to note that pilot applies different techniques depending on type of maneuver and required agility, varying from gentle inputs (fine tracking) up to abrupt stick deflections.

After all cited steps of model validation, the integrated model in flight simulator has achieved a representative level of fidelity to conduct several studies, such as study of Loss of Control In-flight or study of Pilot-Induced Oscillation due to rate limiting (documented for example in Gripp et al. (2023b)).

Figure 10 depicts an example of LOC-I study, checking the behavior of a designed recovery control law. Starting from a trim condition (Flaps=30deg, Calibrated Airspeed=130kn, Altitude=18kft, Weight=531klb, CG=24%MAC), pilot smoothly commands nose up to reduce airspeed at a rate of 1kt/s approximately. As result, angle of attack ($\alpha$) increased along time up to certain value called "$\alpha$ ON" which is the value that triggers a control law to recover the aircraft and protect from stall (indicated by third plot of Figure 10). In this example a recovery control law was programmed to detect the scenario of loss of control and actuate as soon as possible to avoid the stall, in this case applying full elevator deflection to force aircraft nose down.

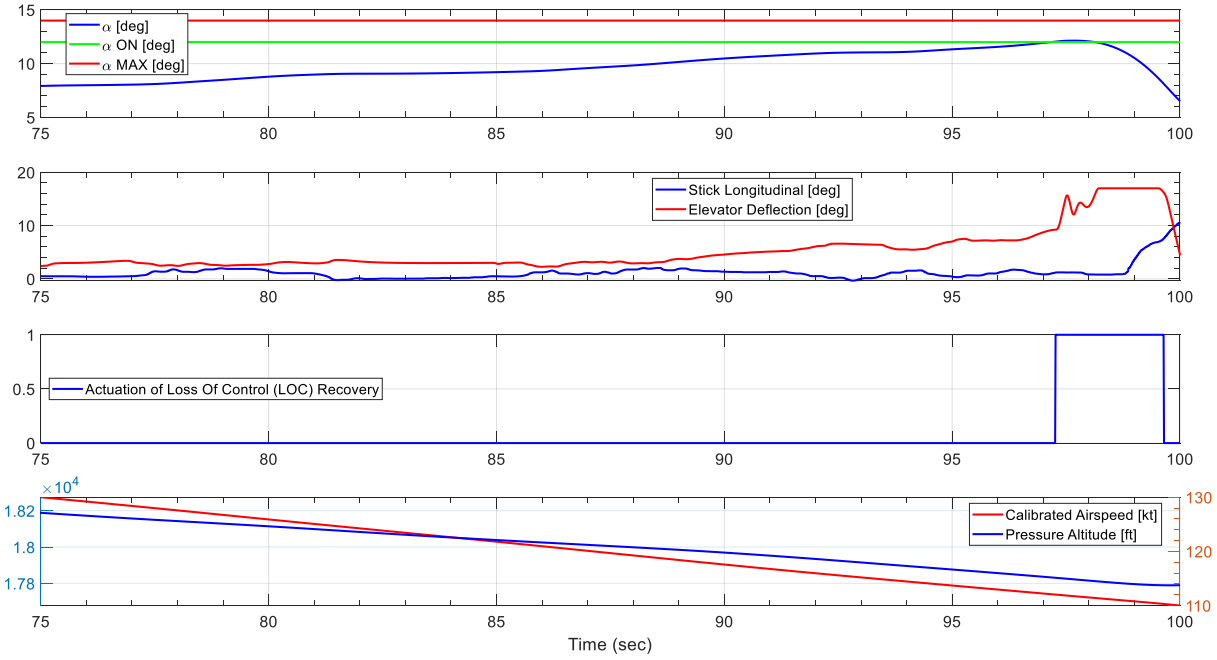


**Figure 10 – Evaluation with pilot-in-the-loop using integrated model: Recovery in case of Loss of Control (LOC).**

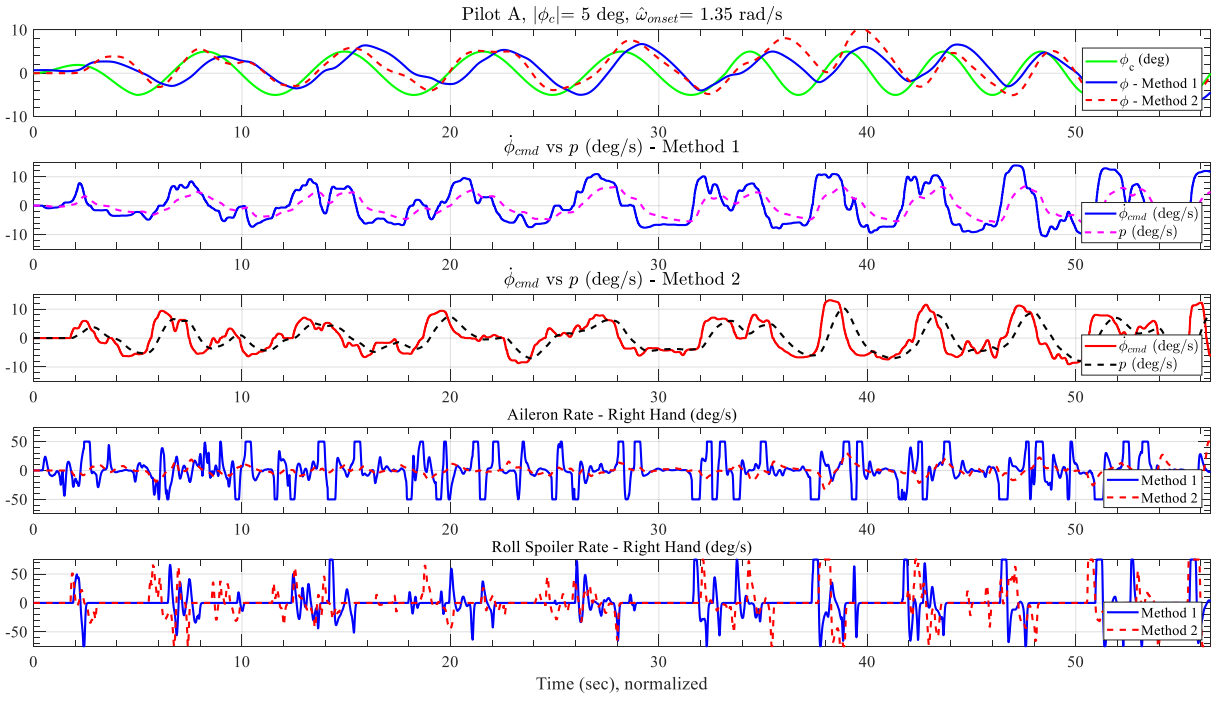


**Figure 11 – Evaluation with pilot-in-the-loop using integrated model: Investigation of PIO due to rate limiting.**

Figure 11 depicts an example of PIO study due to rate limiting in aileron. Starting from a trim condition (Flaps=30deg, Calibrated Airspeed=100kn, Altitude=3kft, Weight=350klb, CG=33%MAC), a sinusoidal tracking reference ($\phi_c$) was presented on the PFD for pilot to track, as illustrated in Figure 7. The sinusoidal reference has amplitude 5 deg and frequency changing from 0.94rad/s (5 cycles) up to 1.35rad/s (more 5 cycles). In this study, $\omega_{onset}$=1.35rad/s is called onset frequency, the frequency at which actuator saturation occurs for the first time in this example (value obtained from offline simulation). Two versions of "p-Beta" control laws (called Method 1 and 2) were tested for same sinusoidal reference, so the pilot could check the tendency of PIO in each case. Each version of p-Beta has different control allocations for aileron and roll spoilers: Method 1 deflects only ailerons for small lateral commands and aileron plus roll spoilers in case of large commands; Method 2, on the other hand, deflects aileron and roll spoilers always together, sharing the efforts, and alleviating the ailerons.

First plot of Figure 11 shows the tracking reference ($\phi_c$) and the aircraft roll angle ($\phi$) in each case of p-Beta control law. Second and third plots from Figure 11 check capacity of aircraft to follow the command reference, where $\dot{\phi}_{cmd}$ represents pilot command in terms of roll angle derivative and $p$ is the aircraft roll rate. Finally, analyzing fourth and fifth plots of Figure 11, it is noticeable that Method 1 has more occurrences of aileron rate saturation if compared to Method 2, indicating that Method 1 is more exposed to PIO due to rate limiting. Gripp et al. (2023b) presents further documentation about this study.

## CONCLUSIONS

This paper presented the main steps of configuration of an aerodynamics model in flight simulator to investigate for example Pilot-Induced Oscillations (PIO) and Loss of Control (LOC), starting from model build-up in Simulink, offline validations with references, integration of models in flight simulator, up to validations with pilot-in-the-loop. Based on a mature environment for simulation, several tests can be performed, such as evaluations of flight control laws to avoid PIO and LOC.

The integration of models such as presented requires time, dedication, organization, adequate tools, and validation of each step in order to converge to a reliable model. However, each model might require particular configurations which are empirically determined (no available references), such as calibration of force for pilot stick, position of projectors for visual cues, indications on the PFD, just to cite examples.

It is important to note that the process conducted in this work can be repeated for other aircraft, and the cases of study are not limited to PIO and LOC. The process of setup of aerodynamics models presented in this paper allows that flight simulators, such as SIVOR platform, to be collaborative and flexible for new designs and research. Moreover, flight test pilots have checked successfully the integration, which demonstrates the consistency of the proposed process.

## ACKNOWLEDGMENTS

Special thanks to EMBRAER company and ITA (Instituto Tecnológico de Aeronáutica) for providing infra-structure, tools, and personnel (pilots and engineers) which contributed with the development of this work.

## REFERENCES

Klyde, D. H., McRuer, D. T., Myers, T. T., "Unified Pilot-Induced Oscillation Theory, Vol. I: PIO Analysis with Linear and Nonlinear Effective Vehicle Characteristics, Including Rate Limiting", Wright Lab., WL-TR-96-3028, 1995.

Efremov, A., Efremov, E., and Tiaglik, M., "Advancements in Predictions of Flying Qualities, Pilot-Induced Oscillation Tendencies, and Flight Safety", Journal of Guidance, Control and Dynamics, Vol. 43, No. 1, 2020, pp. 4–14.

USAF. "Military standard - Flying qualities of piloted aircraft", MIL-STD-1797B, 2006.

Boeing Commercial Airplanes. "Statistical Summary of Commercial Jet Airplane Accidents, Worldwide Operations, 1959-2019". 2020. Available at: www.boeing.com/resources/boeingdotcom/company/about_bca/pdf/statsum.pdf

Belcastro, C. "Loss of control prevention and recovery: Onboard guidance, control, and systems technologies", AIAA Guidance, Navigation, and Control Conference Proceedings, 2012.

Silva, E. T., Penna, S. D., Junior, M. A. O. A., Oliveira, W. R., Villani, E., and Trabasso, L. G., "Flight simulator assisted by a robotic motion platform", AIAA SciTech Forum, 2019.

Oliveira, W. R., Matheus, A., Rodamillans, G., Nicola, R. M., Arjoni, D. H., Trabasso, L. G., E.Villani, and Silva, E. T., "Evaluation of the pilot perception in a robotic flight simulator with and without a linear unit", AIAA SciTech Forum, 2019.

NASA, "The Simulation of a Jumbo Jet Transport Aircraft Volume II: Modeling Data", NASA D6-30643, USA, 1970.

Roskam, J., "Airplane Design VI: Preliminary Calculation of Aerodynamic, Thrust and Power Characteristics". DARcorporation, 1985.

RECOVER. "Aircraft simulation benchmark: Reconfigurable control for vehicle emergency return". 2004. Available at: http://www.faulttolerantcontrol.nl. Accessed on: 17 nov. 2019.

Stevens, B., and Lewis, F., "Aircraft control and simulation", John Wiley and Sons, 1992.

Silva, A. S. F. “An approach to design feedback controllers for flight control systems employing the concepts of gain scheduling and optimization”. Masters of Science — Instituto Tecnológico de Aeronáutica (ITA), São José dos Campos, Brazil, 2009.

Moreira, M. A. G., Gripp, J. A. B., Yoneyama, T., and Marinho, C. M. P., “Longitudinal Flight Control Law Design with Integrated Envelope Protection”, Journal of Guidance, Control and Dynamics, 2022.

Gripp, J. A. B., Moreira, M. A. G., Trabasso, L. G., Marinho, C. M. P. “Control allocation to roll fly-by-wire aircraft with ailerons and roll spoilers”, Proceedings to the XIX International Symposium on Dynamic Problems of Mechanics (DINAME), ABCM, 2023.

Gripp, J. A. B., Moreira, M. A. G., Trabasso, L. G., Marinho, C. M. P. “Evaluation of Open Loop Onset Point Criterion to predict rate saturation PIO using flight simulator”, Proceedings to the XIX International Symposium on Dynamic Problems of Mechanics (DINAME), ABCM, 2023.